Widmanst✍tten precipitation; research in progress

(i.e. current status and plans)

Gary R. Purdy, McMaster University

Experiment and Classical Modeling		Phase-field Modelling
Yan Li		*Nikolas Provatas*
Marc Bletry	←········	*Michael Greenwood*
Guillaume Lϑquippϑ		

Objective: "evaluation of the roles of interfacial energy, elastic energy, diffusion and interface mobility in the formation of Widmanst≅tten precipitates."

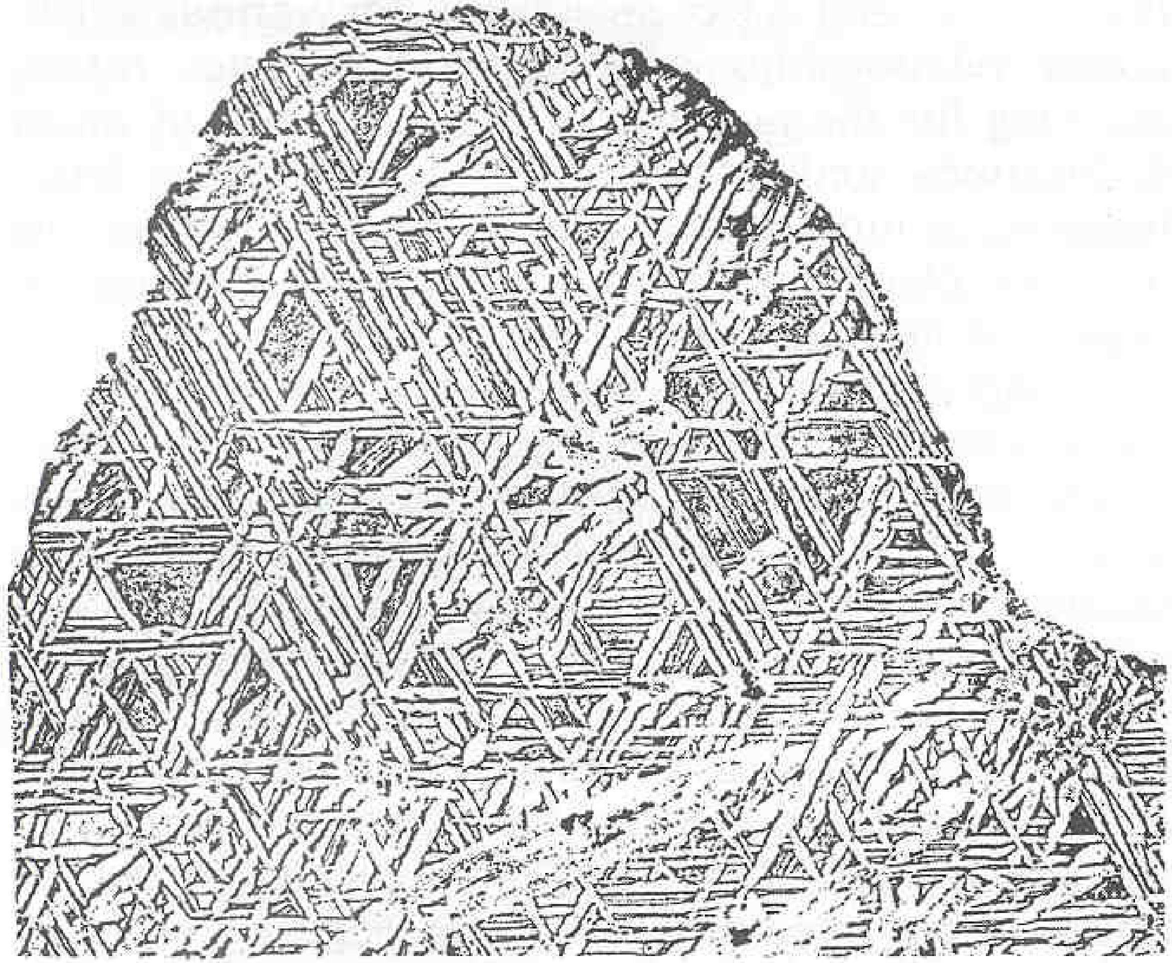

Typographical image of the Elbogen iron meteorite,
after von Schreiber (1820)

Systems under study:

1. θ' in α Al-Cu (intergranular)
   Well characterized, sharply defined crystallography.

2. α in β Cu-Zn (intragranular origin)
   fcc/bcc; analogue of transformation in steels.

3. α in γ Fe-C-X (to be developed)
   Widmanstätten ferrite and bainite

1. θ’ in α Al-Cu

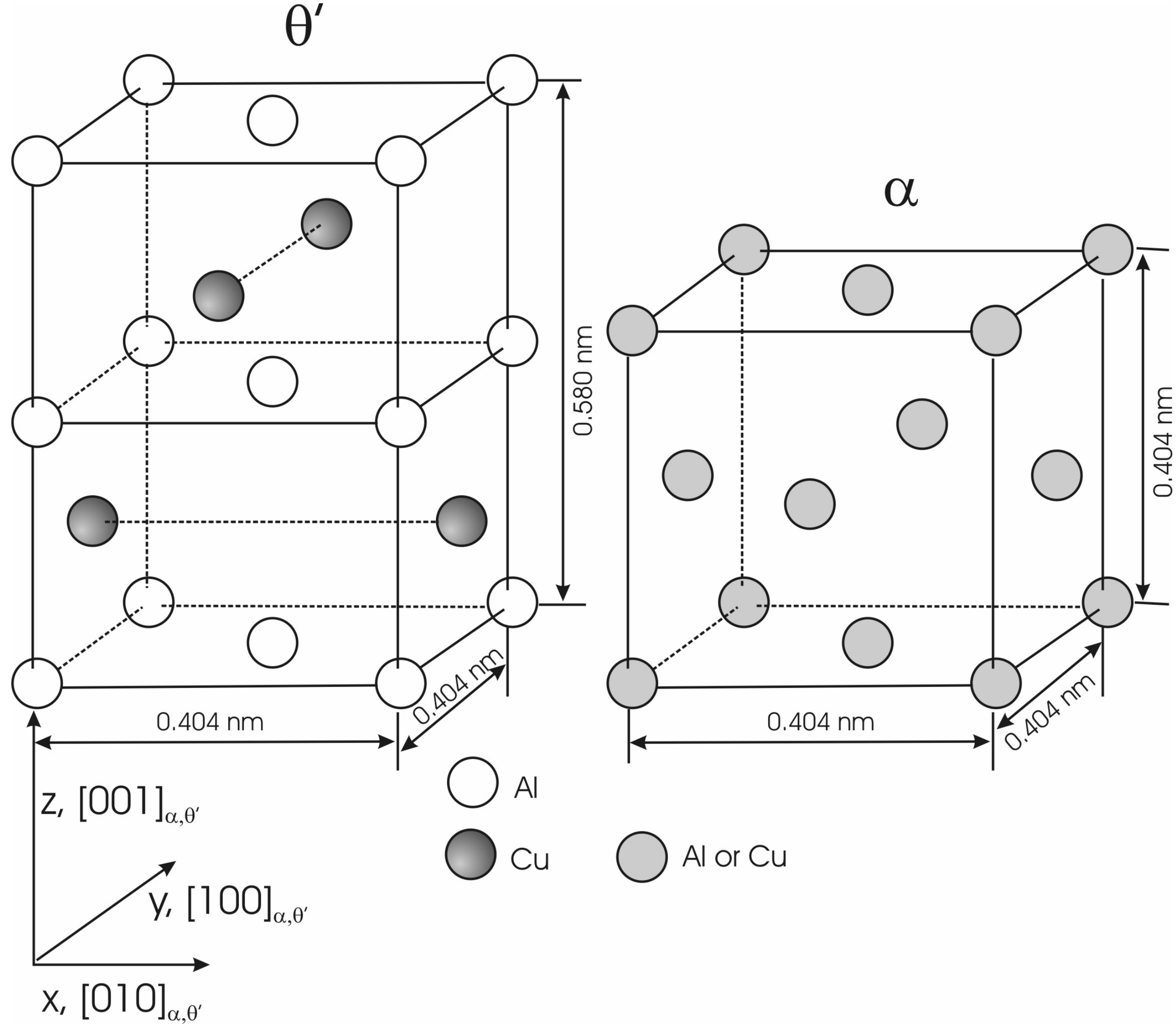
θ′
α
0.580 nm
0.404 nm
0.404 nm
0.404 nm
0.404 nm
0.404 nm
z, [001]α,θ′
y, [100]α,θ′
x, [010]α,θ′
Al
Cu
Al or Cu

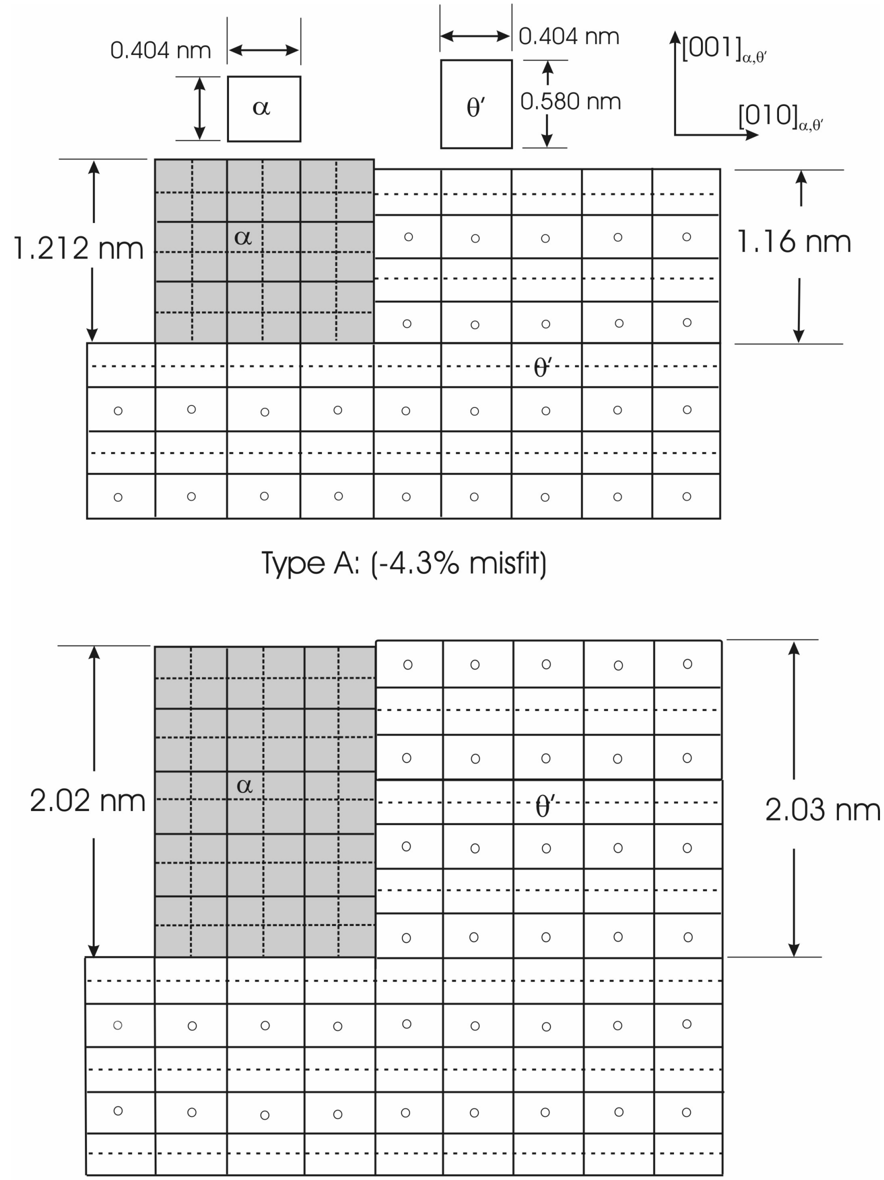

Type A: (-4.3% misfit)

Type B: (+0.45% misfit)

Purdy and Hirth, 2006

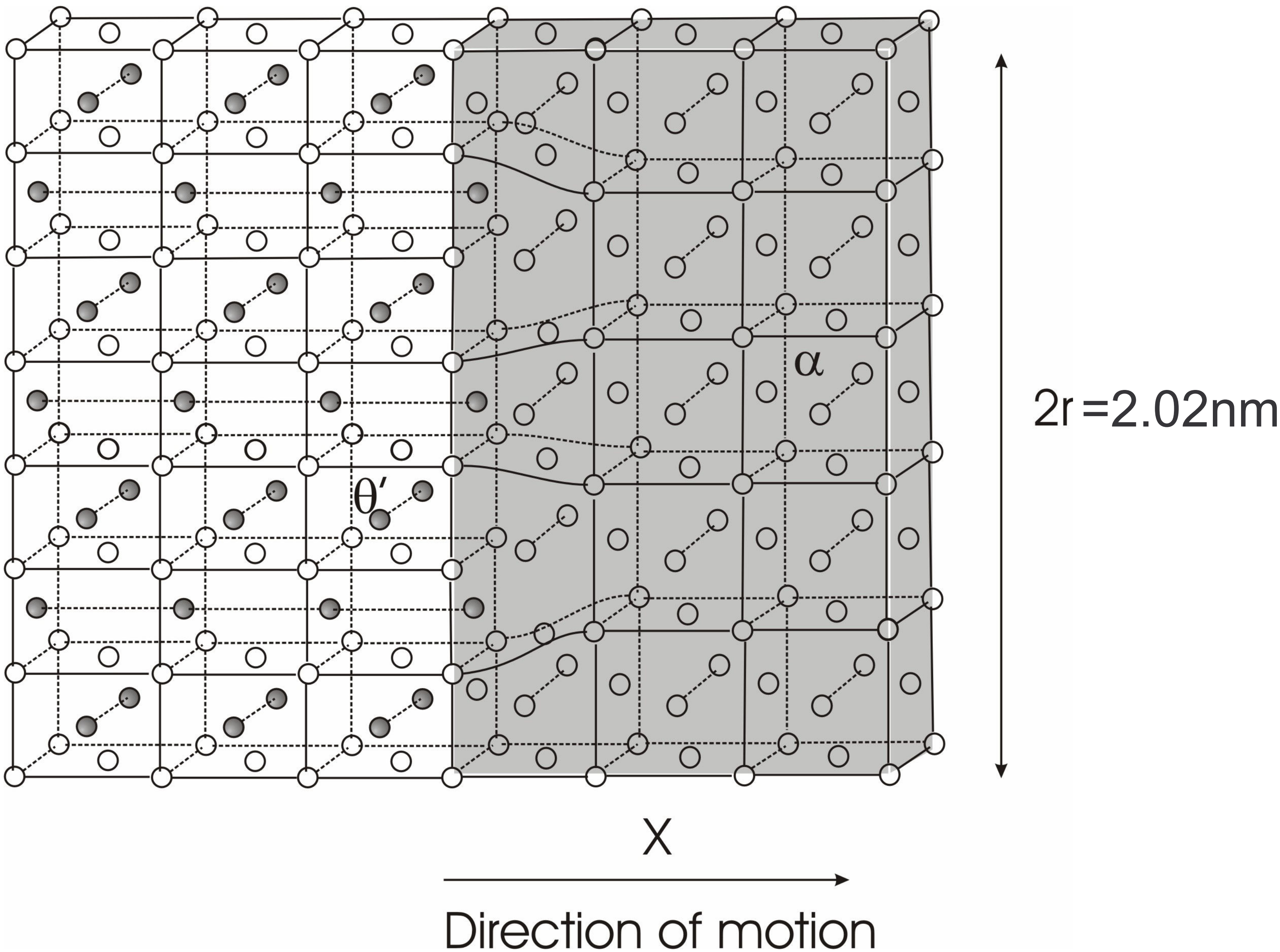
θ′
α
2r =2.02nm
X
Direction of motion

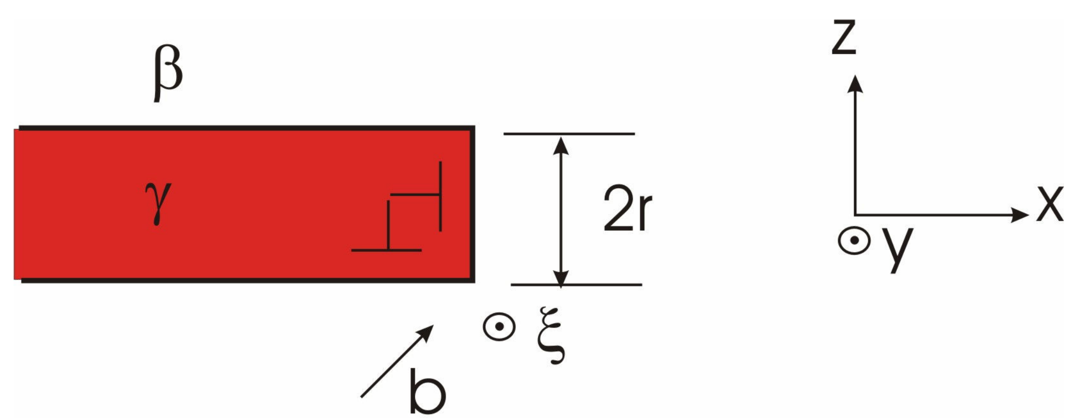

General case,
Plate-like ppt.

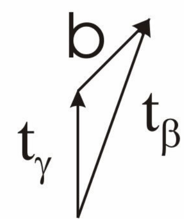

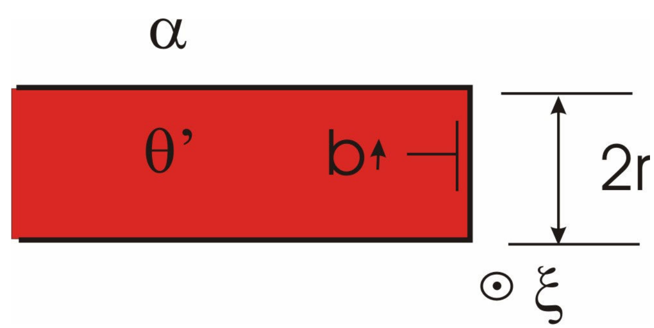

The specific case of θ’ in α Al-Cu

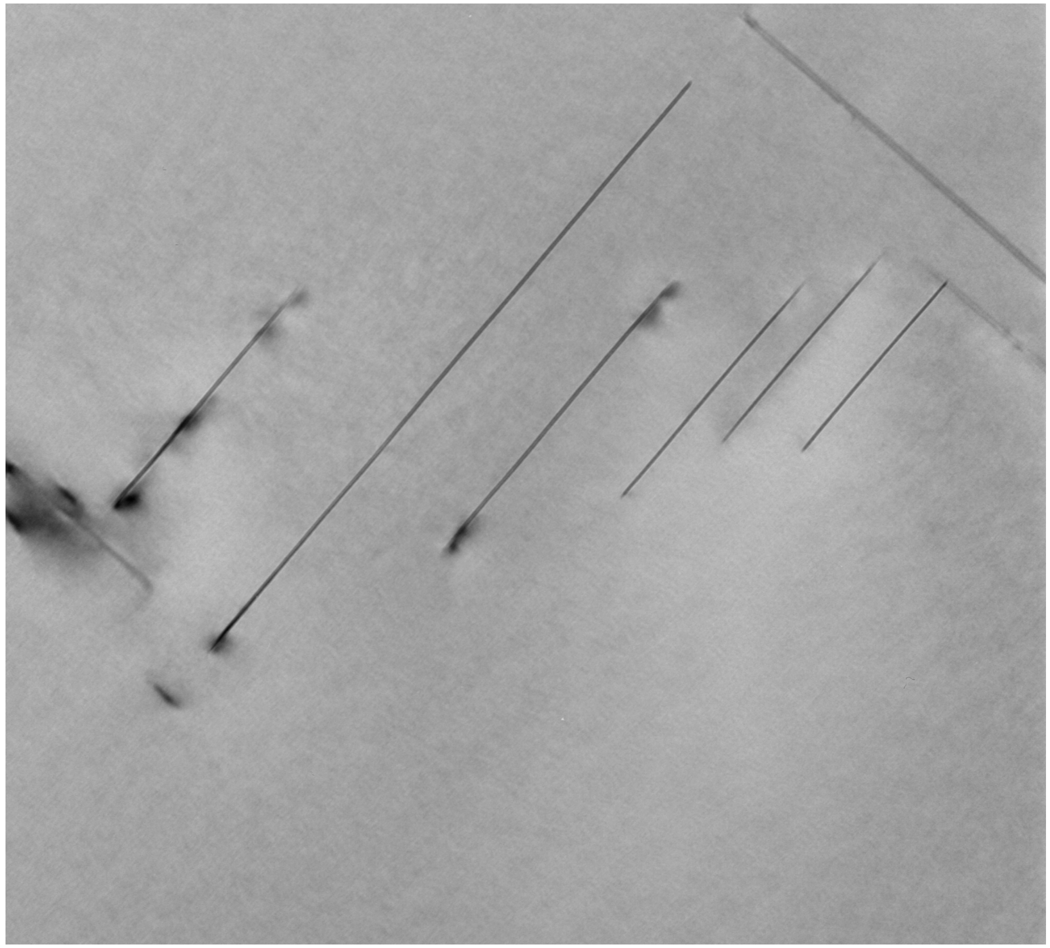

Early stages of θ’ growth in Al-3Cu

Growth kinetics; classical approach.

$$\frac{v}{M} = P_i = P_{th} + P_\sigma + P_{el} + P_{s.d.} + P_Z$$

A local force balance is employed to relate velocity v to a set of forces:

- Intrinsic drag, P_i related to interfacial structure, mobility, M
- A thermodynamic driving force, $P_{th} = \Delta G_{int}/V_m$
- A capillary force P_σ due to interfacial curvature,
- An elastic force, P_{el} due to coherency strains, interactions
- A solute drag force, P_{sd} due to solute diffusion within interface,
- A Zener drag, due to particle interactions with interface.

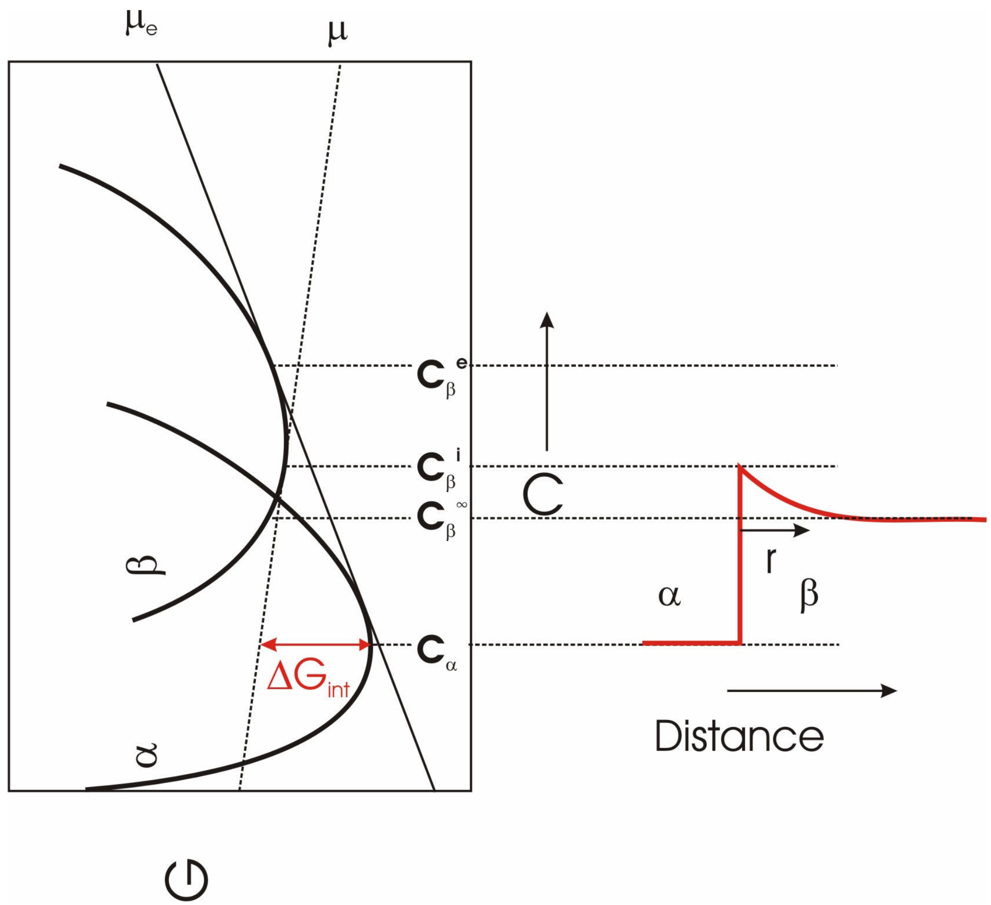

$$f_{th} = \frac{\Delta G_{\text{int}} \cdot 2r}{V_m};$$

Thermodynamic force (per unit length);

$$v \approx \frac{D_\beta}{r} \frac{c_\beta^i - c_\beta^\infty}{c_\beta^i - c_\alpha}$$

Zener-Hillert analysis of steady plate lengthening

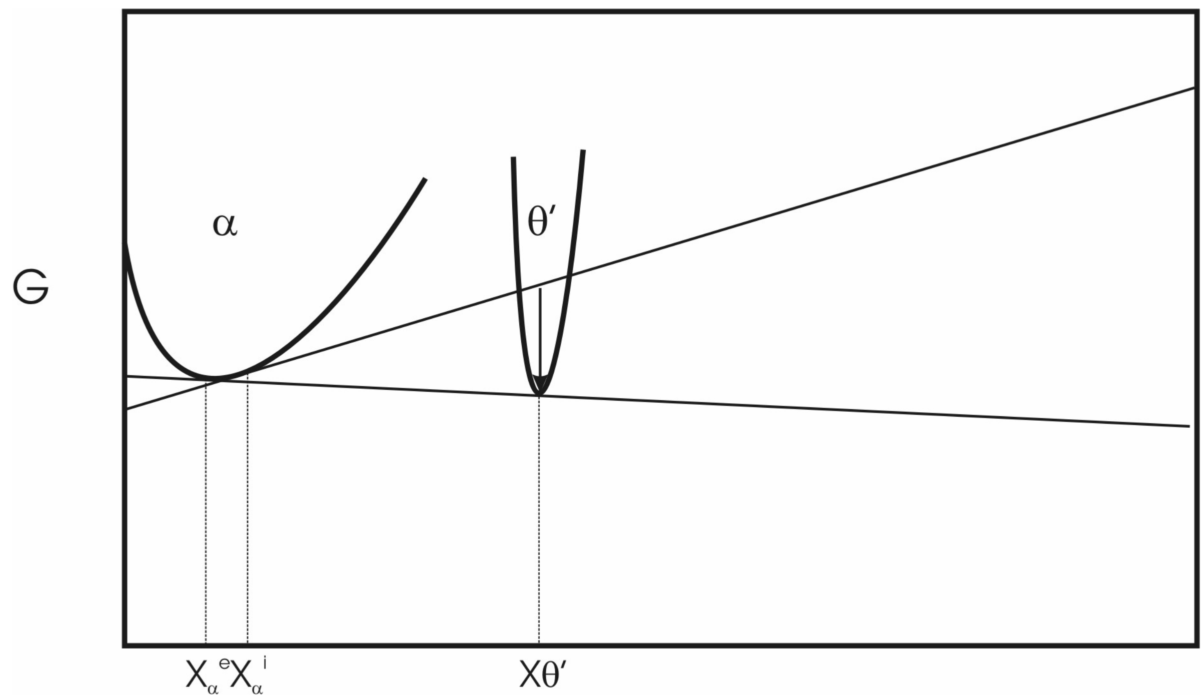
G
α
θ′
$X_\alpha^e X_\alpha^i$
Xθ′

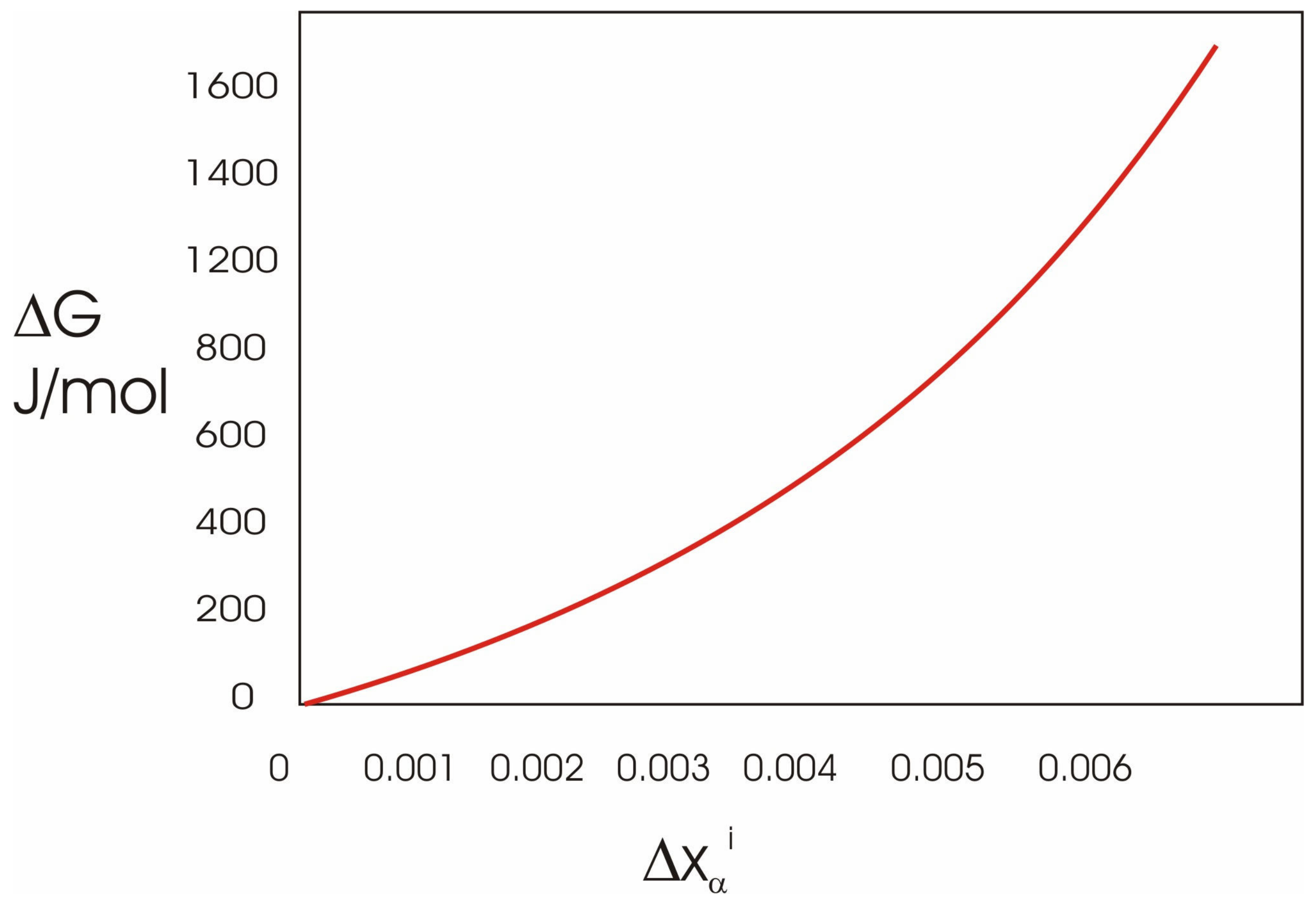
ΔG
J/mol
1600
1400
1200
800
600
400
200
0
0
0.001
0.002
0.003
0.004
0.005
0.006
Δx α i

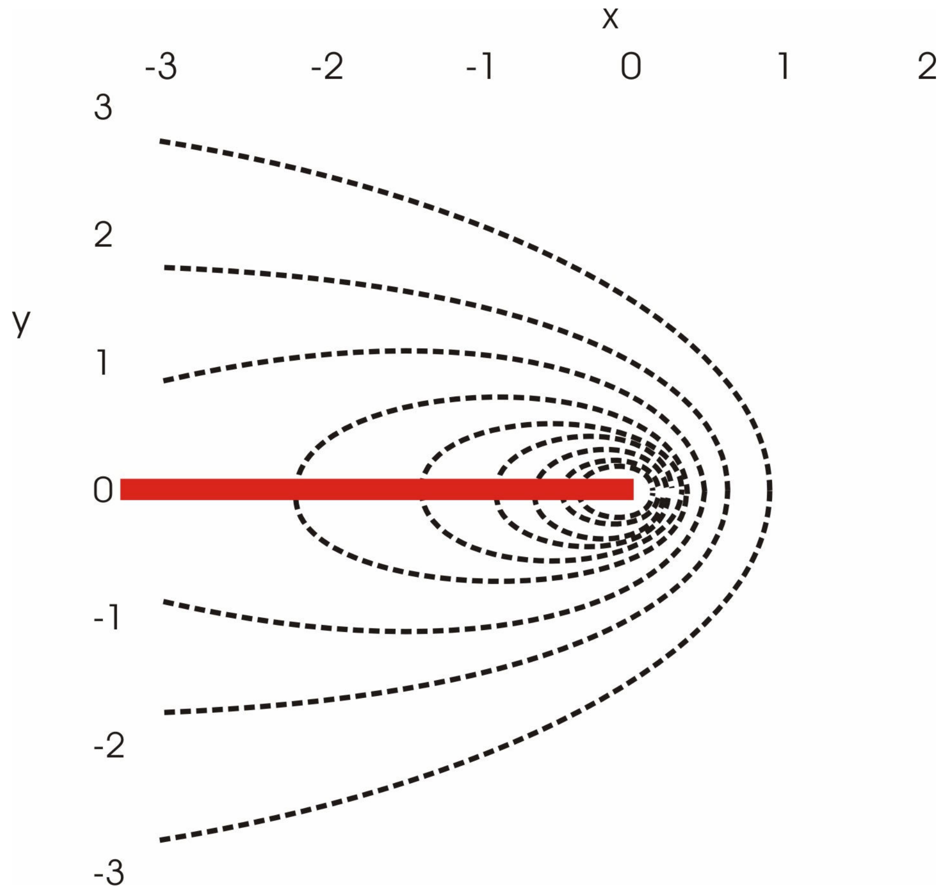

$$c(x,y) = \frac{c_\beta^i}{K_0\left(\frac{vb}{2D}\right)} e^{-vx/2D} K_0\left\{\frac{v}{2D}(x^2+y^2)^{1/2}\right\}$$

Force/unit length on a migrating θ' edge due to atomic misfit in the diffusion field:

$$f_x = \frac{\partial^2 \Psi}{\partial x^2} \approx -2\mu\eta(c_\beta^i - c_\beta^\infty)\left\{1 + \frac{2.3}{K_0\left[\frac{vb}{2D}\right]}\right\}$$

μ: shear modulus of matrix

η: $= \frac{d \ln a}{dc}$

b: Burgers vector

Self strain energy:

$$E_{el} = \frac{1}{2}\varepsilon_{ij}\int_{v}\sigma_{ij}dv$$

$$f_{el} = \frac{dE_{el}}{dx}$$

Capillary term:

□ $2\sigma_{coh}$

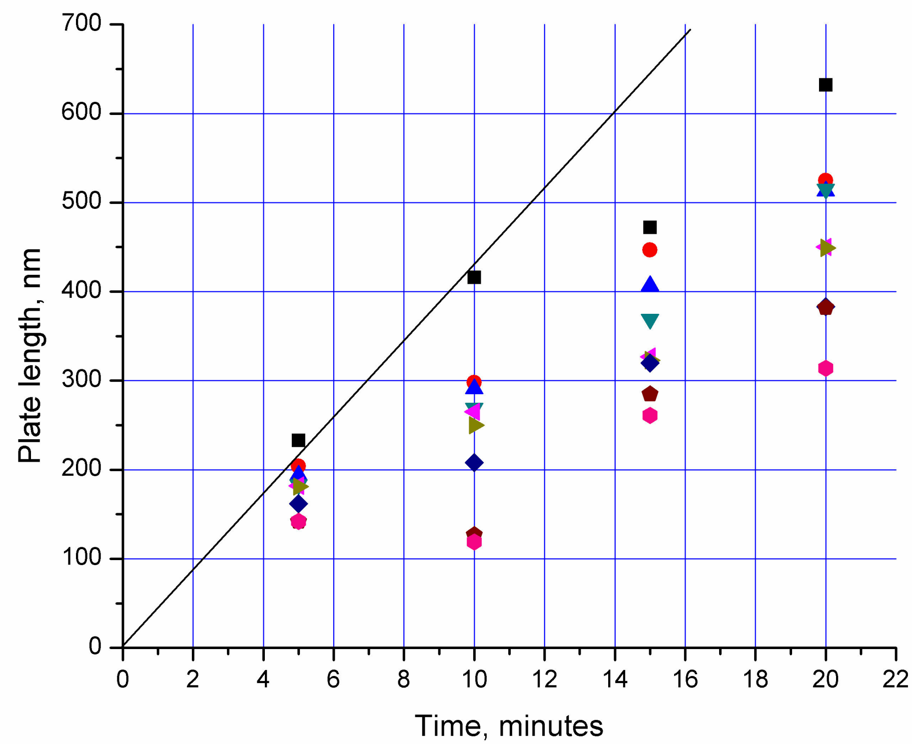

Lengthening kinetics, 2 nm plates
≅20 nm/min

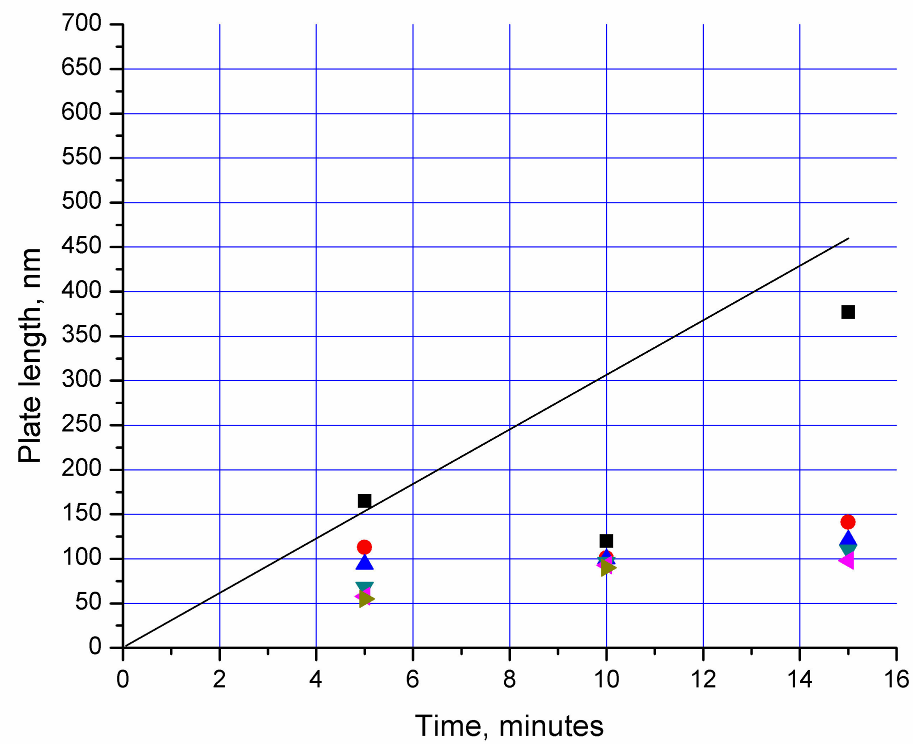

Lengthening kinetics, 1.2 nm plates
≅15 nm/min

Plans for further investigation of θ' precipitation:

- Complete growth kinetic studies, lengthening rate and (simultaneous) thickness measurements.

- Modelling, preliminary procedure and results:
  - Comparison of 2 nm and 1.2 nm plate lengthening;
  - Improved model of velocity vs c_β^i via finite element routine.
  - 2 nm plates are essentially stress-free; fit equilibrium solubility and D to observed 20 nm/min rate.
  - 1.2 nm plates are accompanied by large self-stress, coupling between **b** and solute field (smaller);
  - Extreme sensitivity of 1.2 nm result to elastic terms.

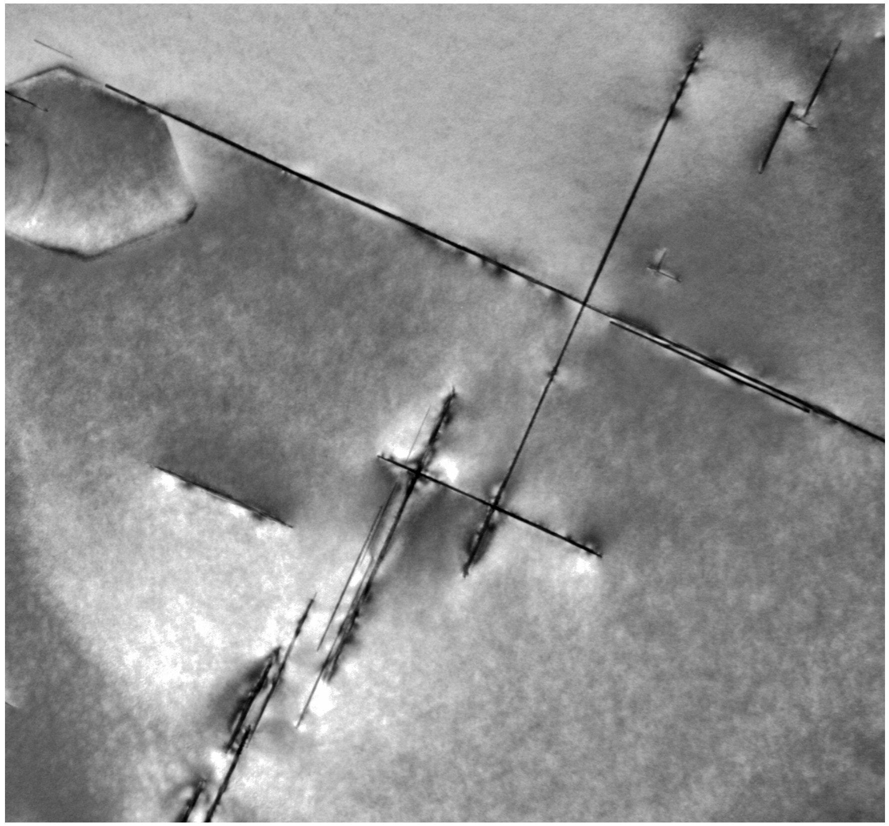

θ' plate intersections

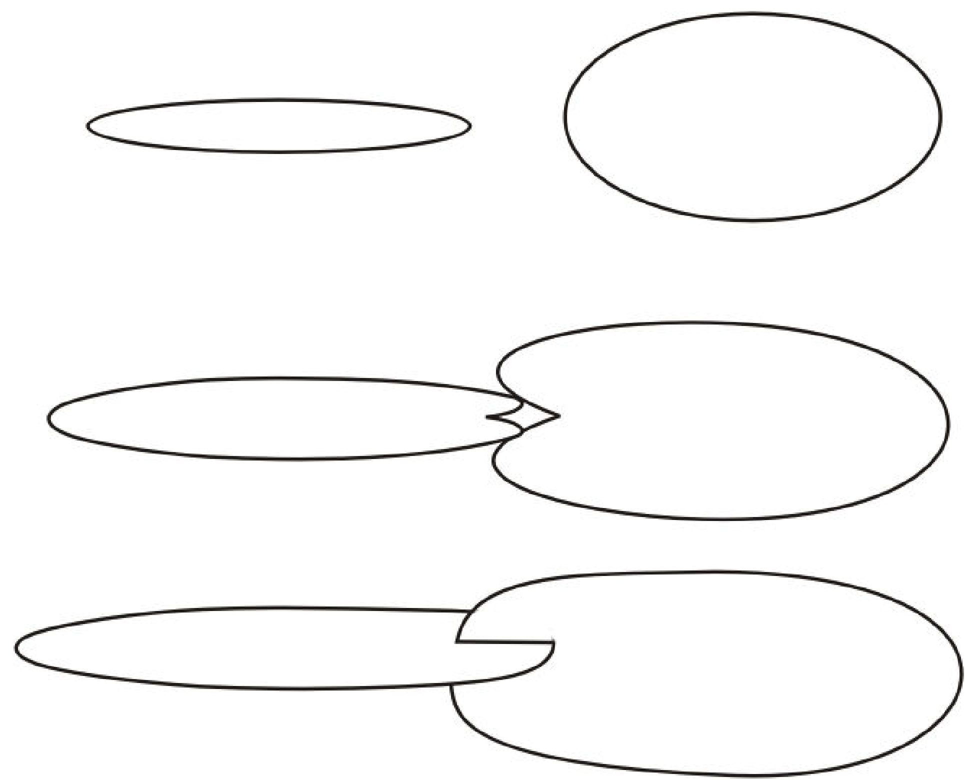

Plate intersections, proposed mechanism

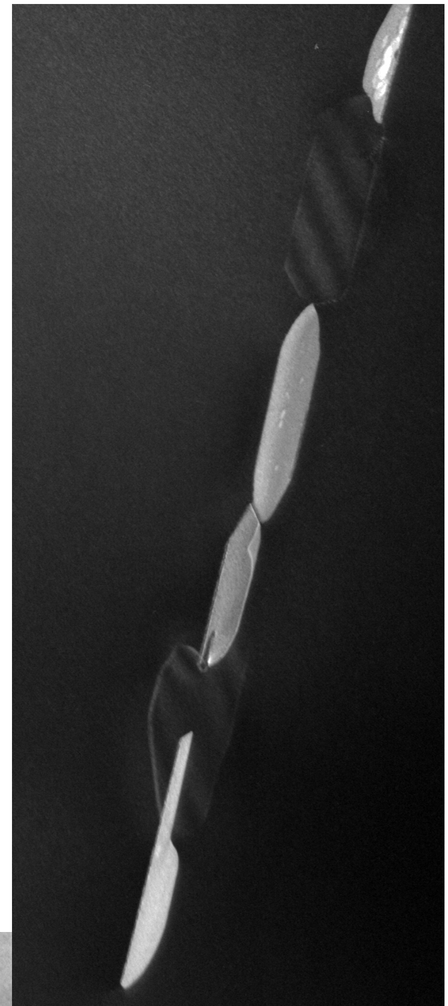

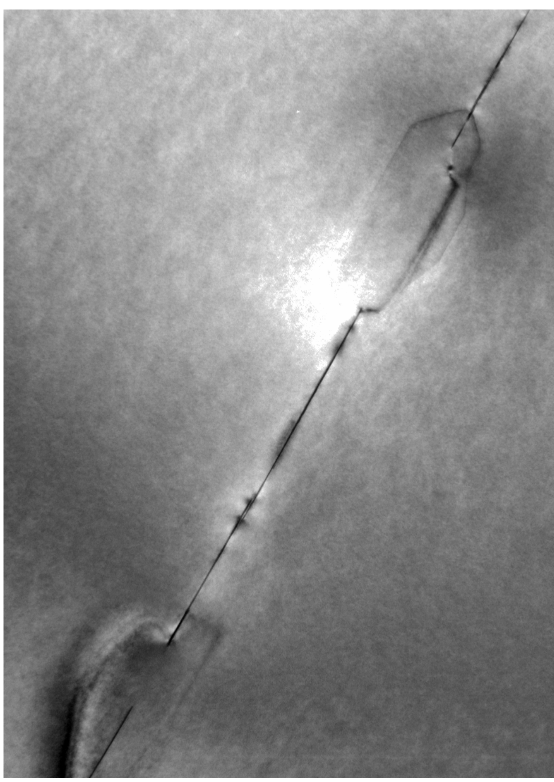

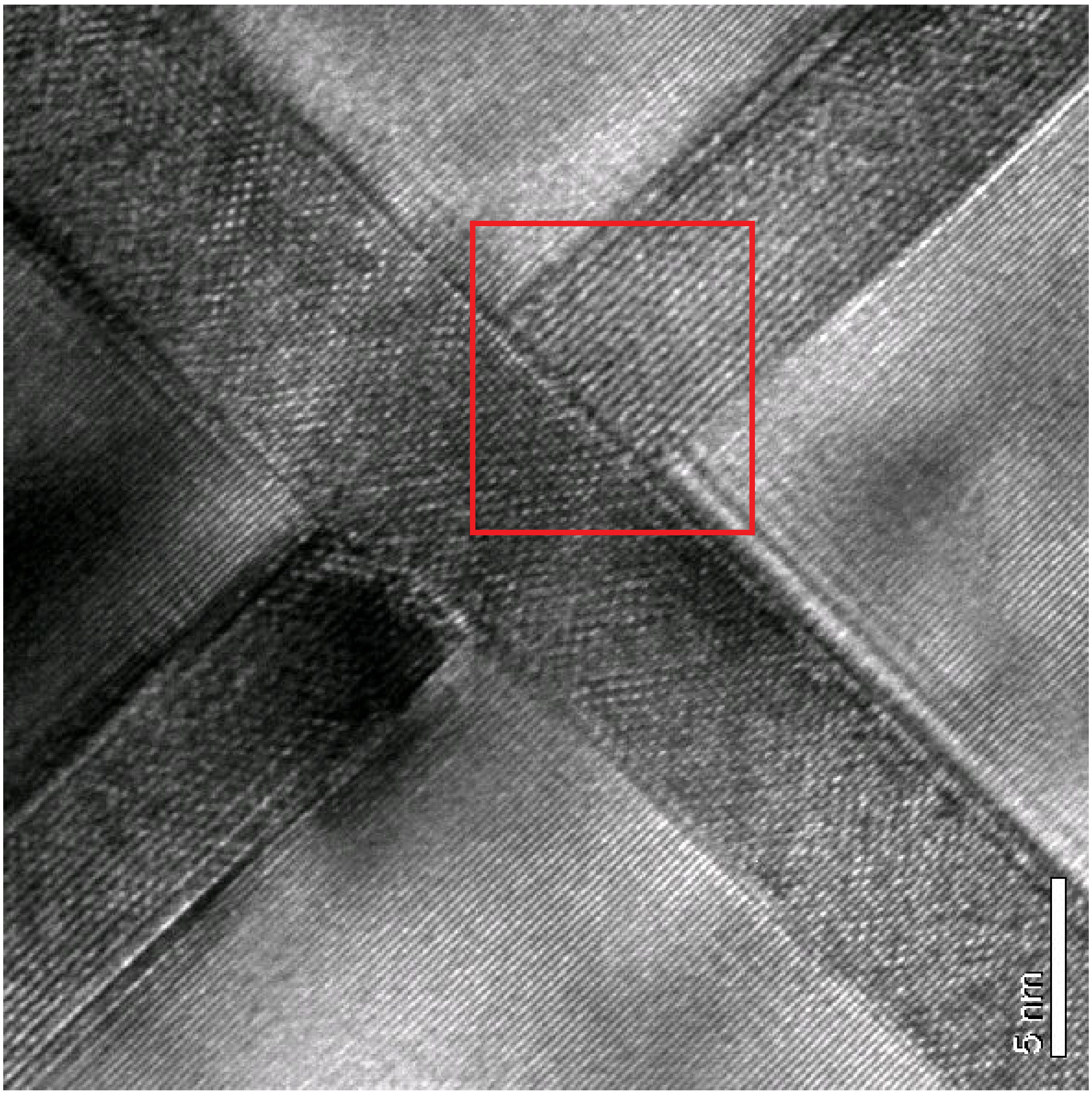
5 nm

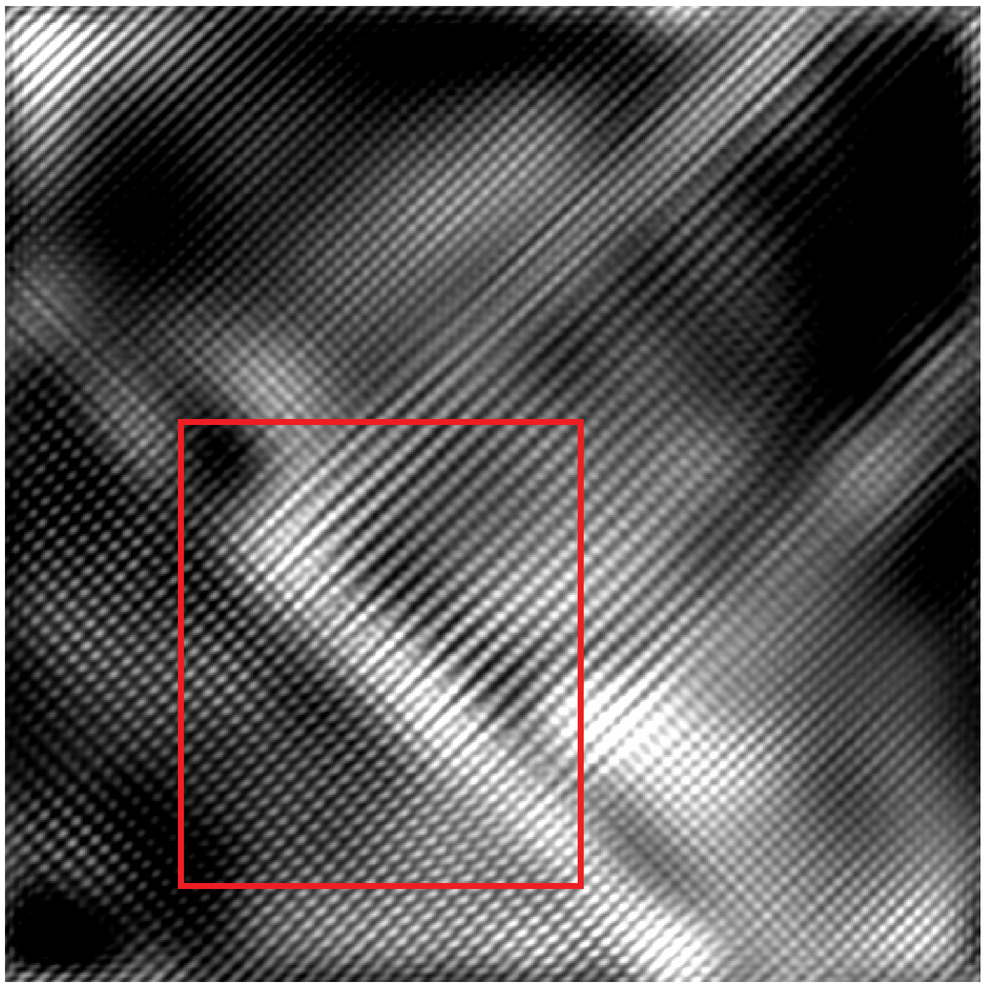

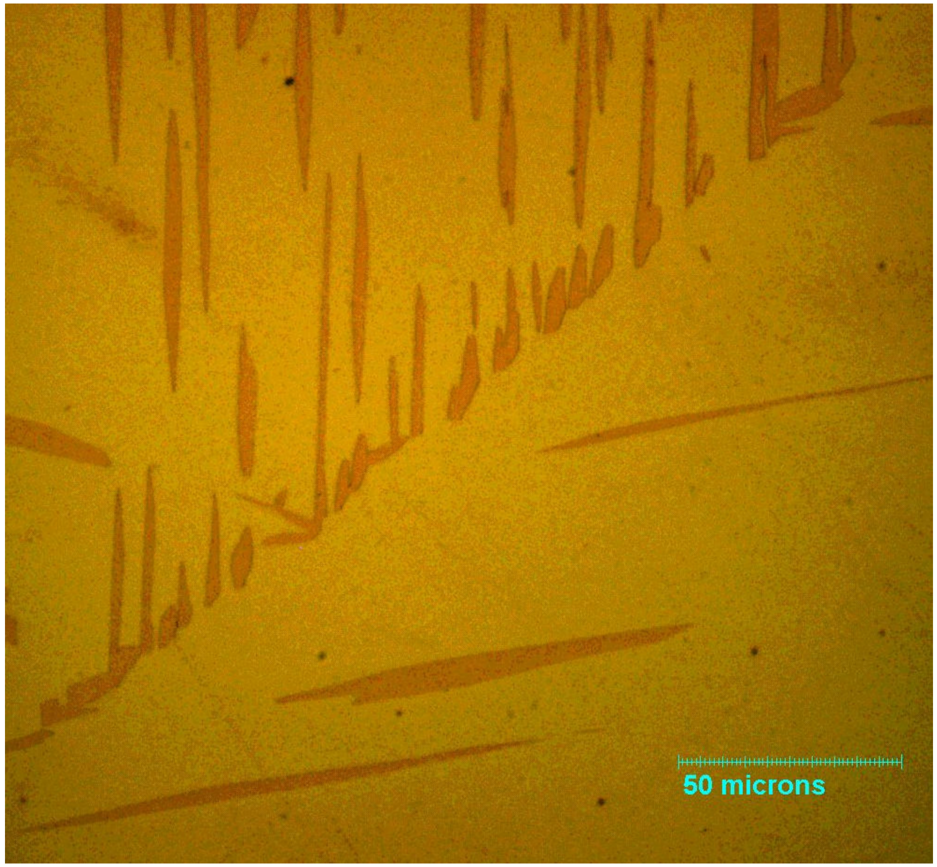

2. α (f.c.c) in β (b.c.c.) brass, kinetics and crystallography

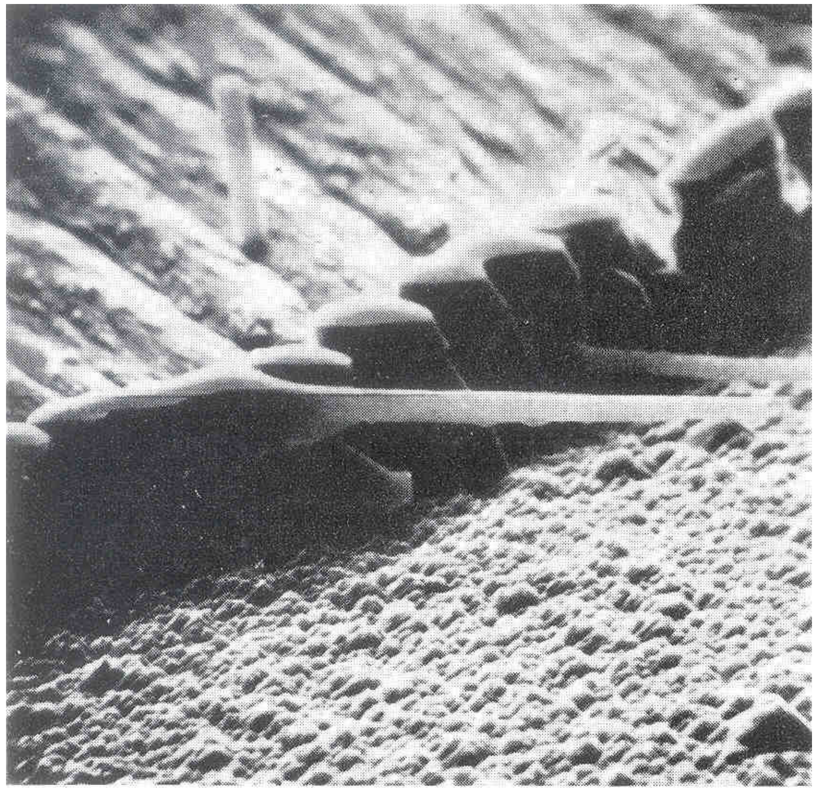

Deep etching; α needles, Cu-0.441 Zn

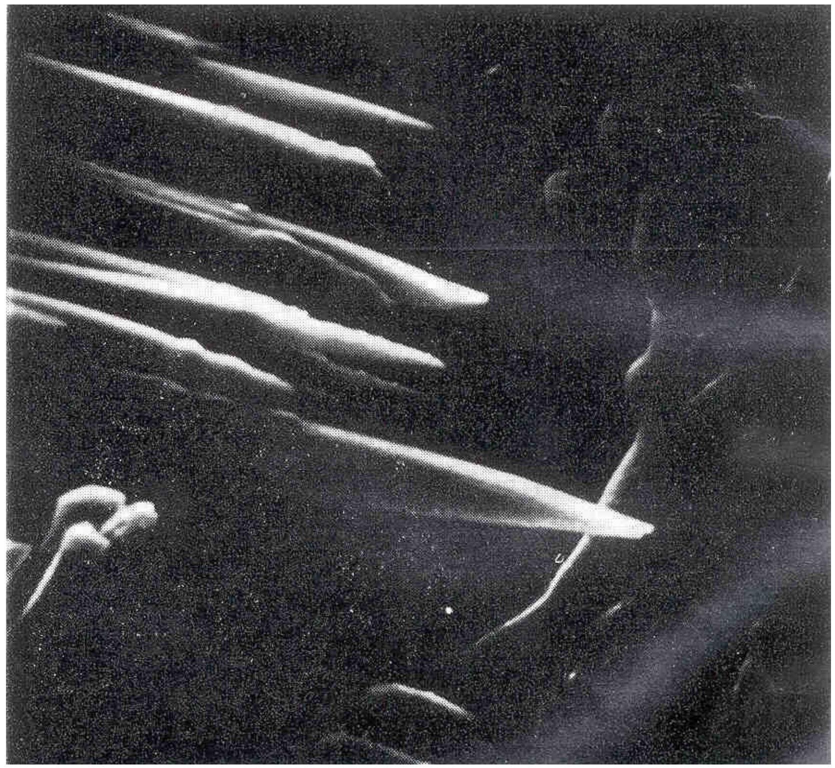

Widmanstätten needles in Cu-0.441Zn,
$T = 400^{o}C$, $v \approx 0.15 \mu m/s$, $r \approx 0.1\ \mu m$

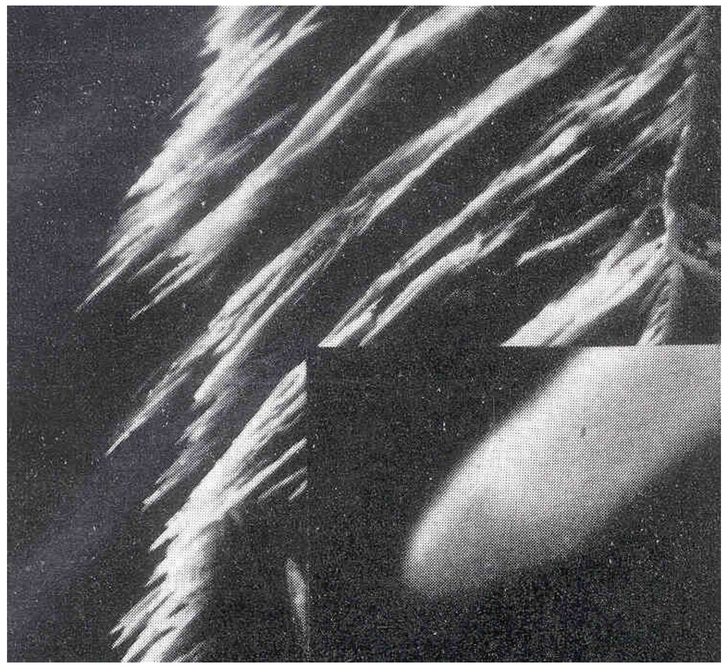

Higher supersaturation; Cu-0.411 Zn

$T = 400^{o}C$, v 📫 5 μm/s, r 📫 0.05 μm

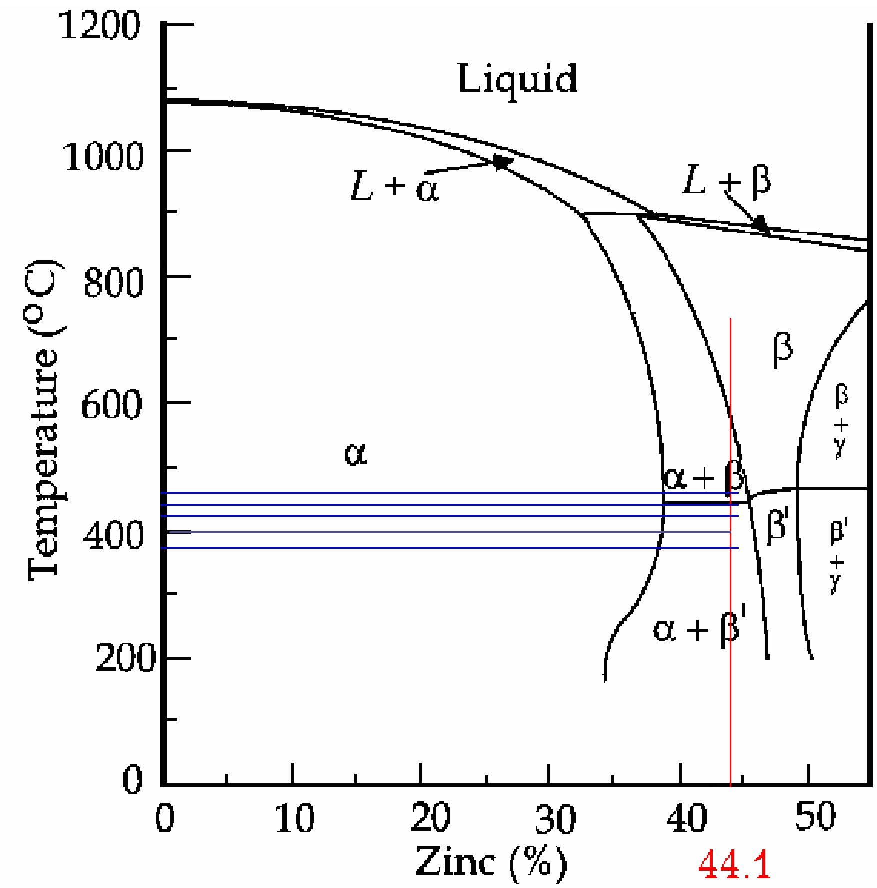
Liquid
L + α
L + β
α
β
β + γ
α + β
β'
β' + γ
α + β'
Temperature (°C)
1200
1000
800
600
400
200
0
0
10
20
30
40
50
Zinc (%)
44.1

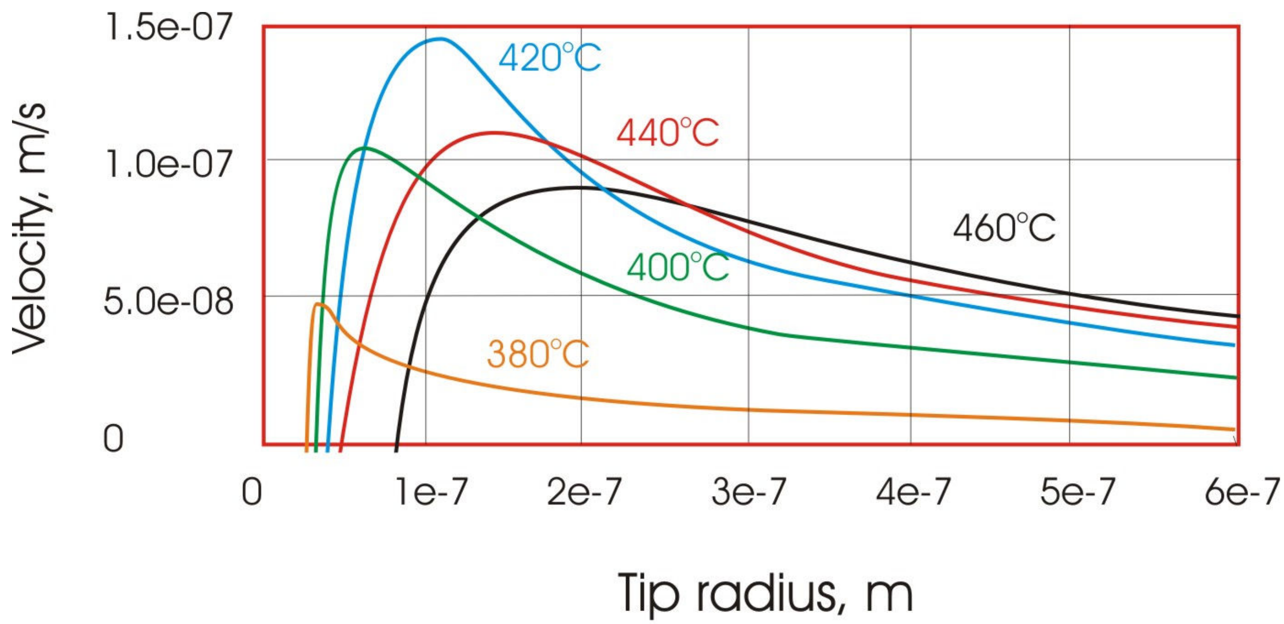

Estimated v vs r relationships for Cu-0.441Zn,
using Zener-Hillert relationship

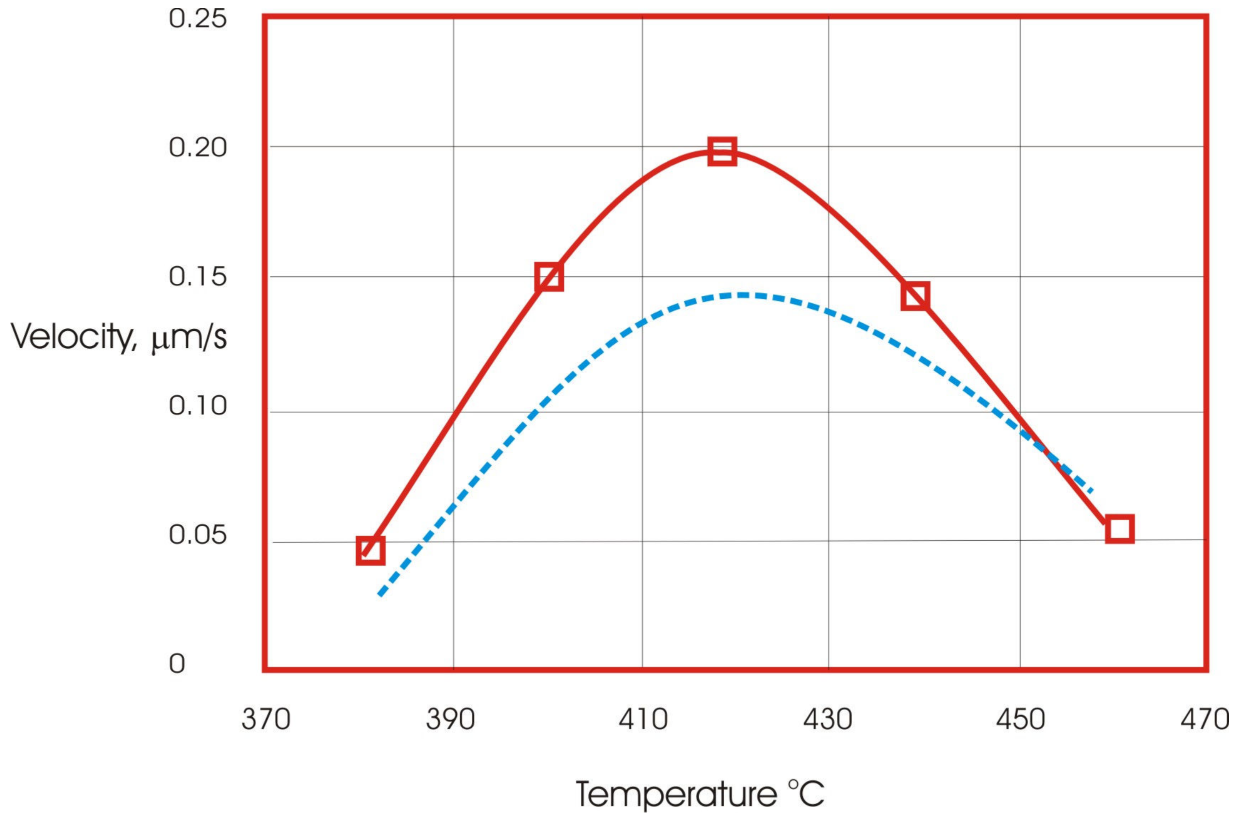

Calculated v_{max} vs experiment

Cu-0.441Zn

Multi-Scale Modeling of Solidification: Phase-Field Method

Field of the Phase in terms of an order parameter

Order Parameter $\quad -1 < \phi < 1$

$\phi = +1 \Rightarrow$ solid $\quad \phi = -1 \Rightarrow$ liquid

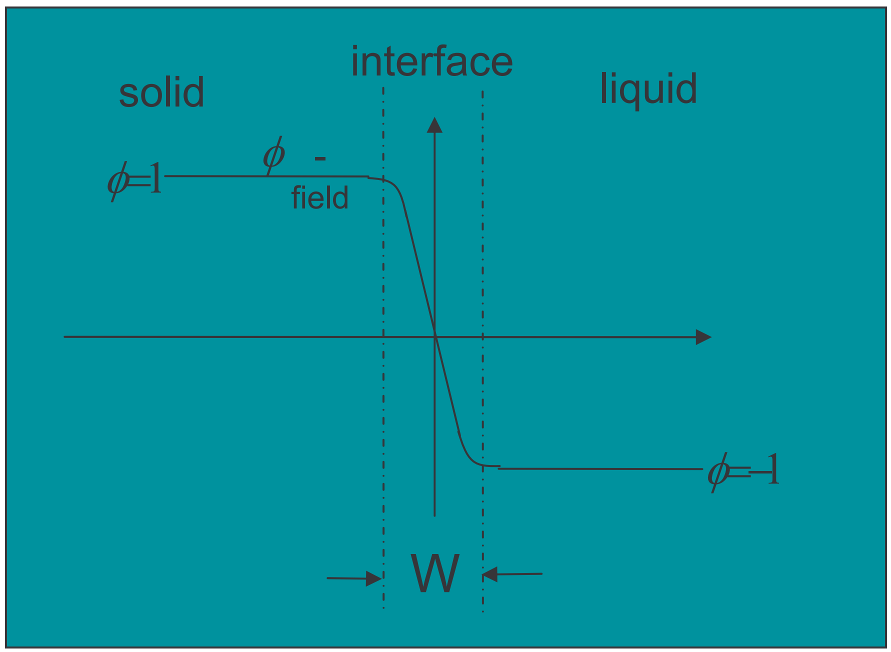

Needle and Dendrite Tip Comparison

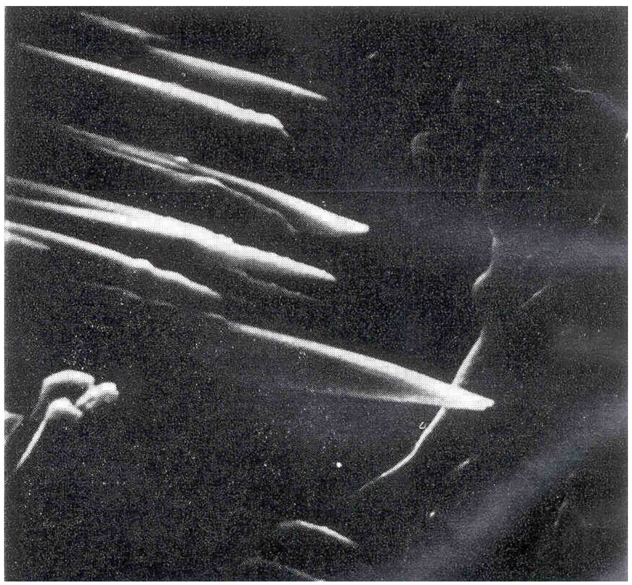

Electron Micrograph of
Alpha Cu-Zn Needle Tips

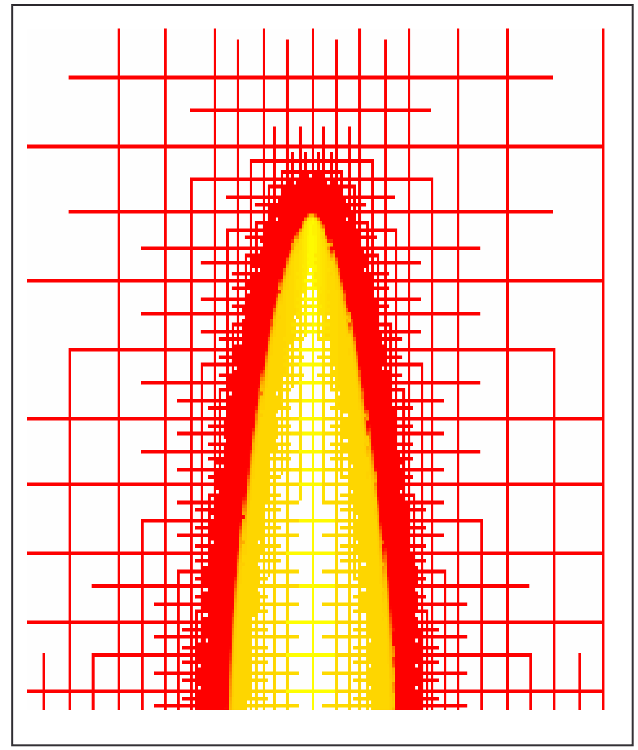

Tip of Phase Field Dendrite

Overall Shape is different, but the tip shapes are similar

Normalized Velocity Comparison

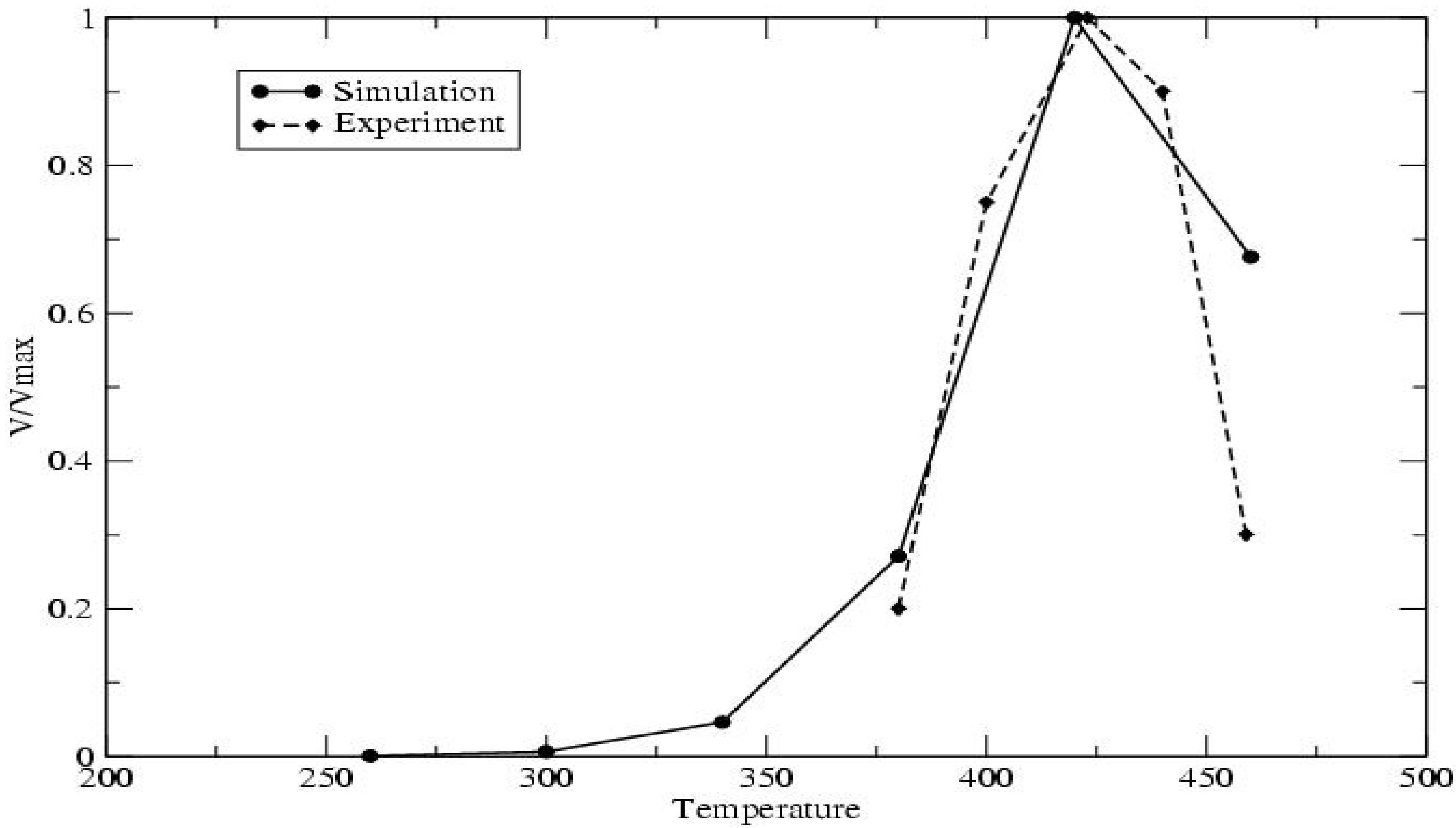

- Good agreement with experiments
- Suggests that the morphology of the needle as a whole has little effect on the rate of growth at the tip.

Orientation imaging of Widmanstätten precipitates:

Proeutectoid cementite from austenite;

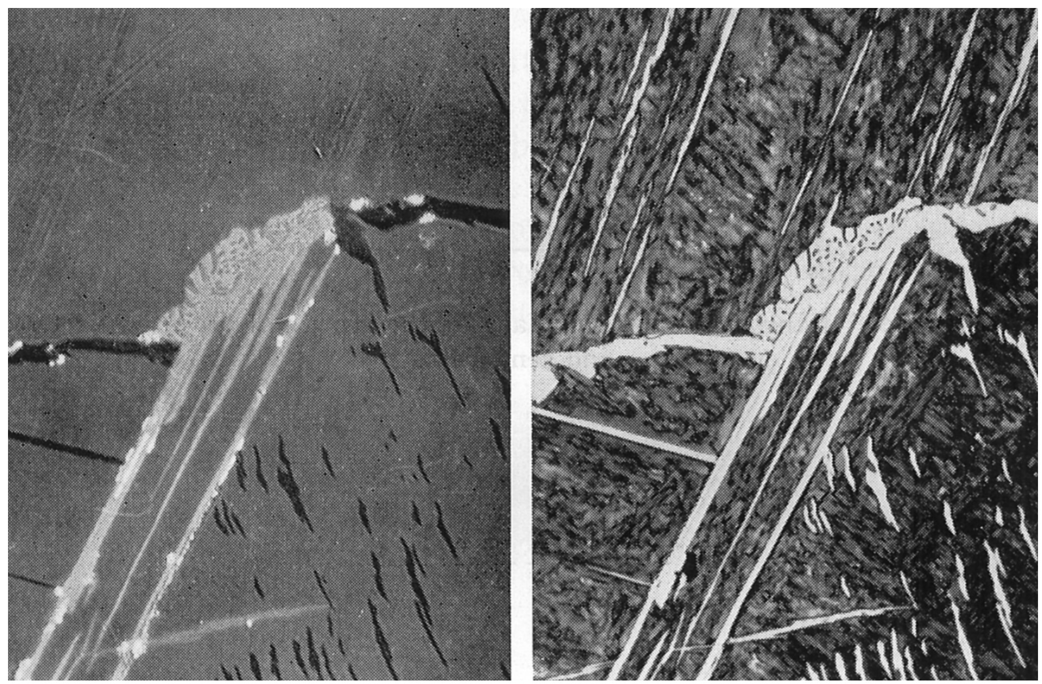

Mats Hillert, 1964

α in β brass; crystallography of grain boundary precipitation.

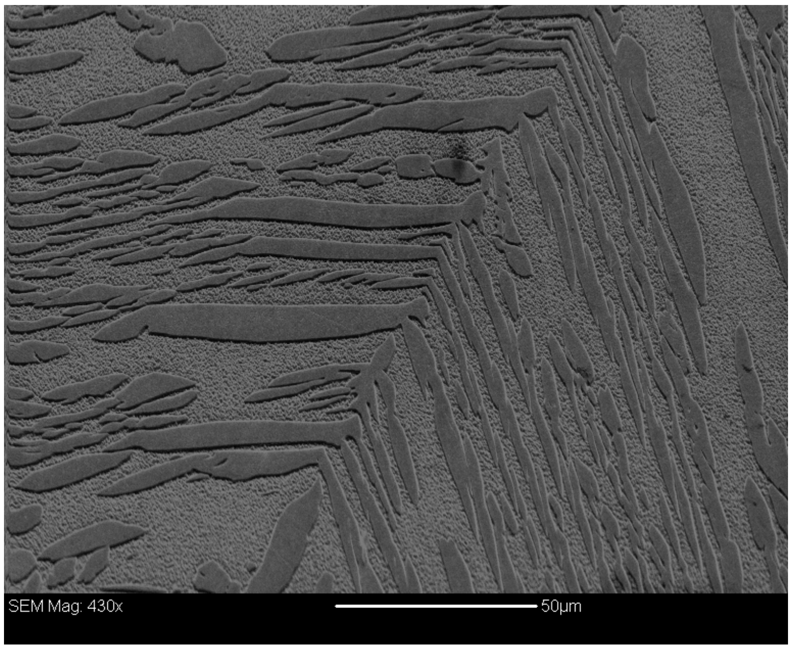

SEM image

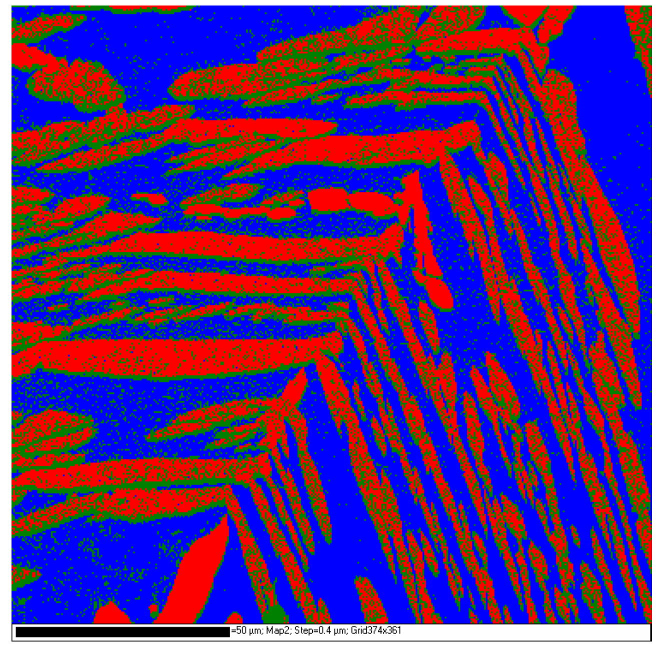

Phase identification

α, β

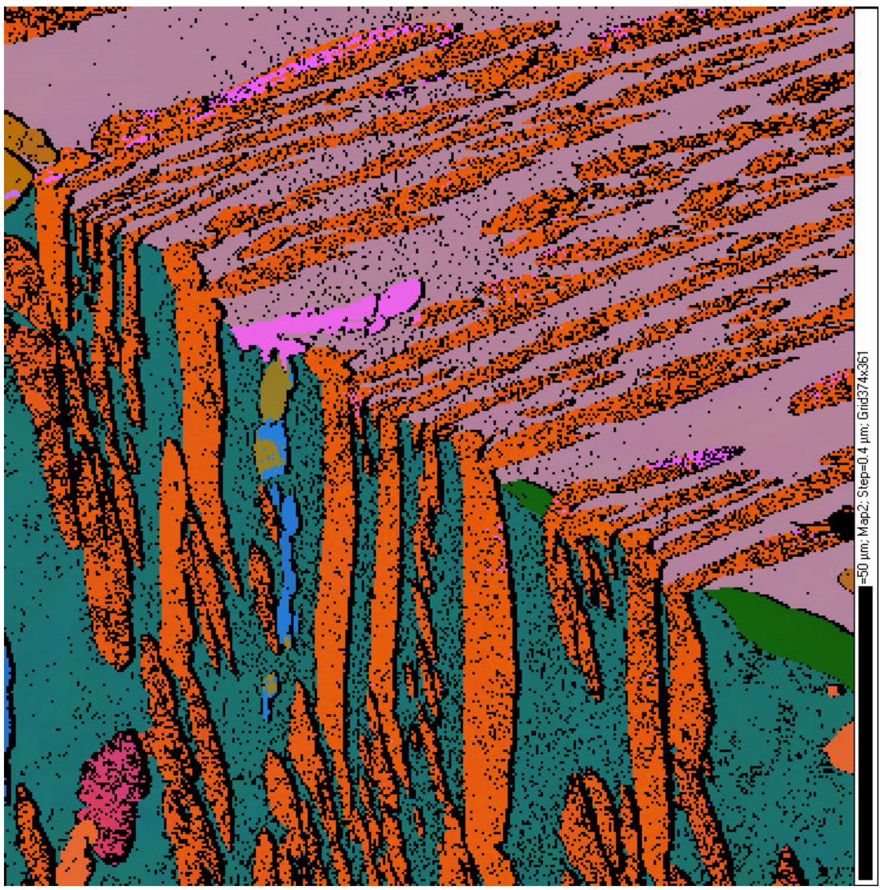
=50 µm; Map2; Step=0.4 µm; Grid374x361

Phases, α, β brass

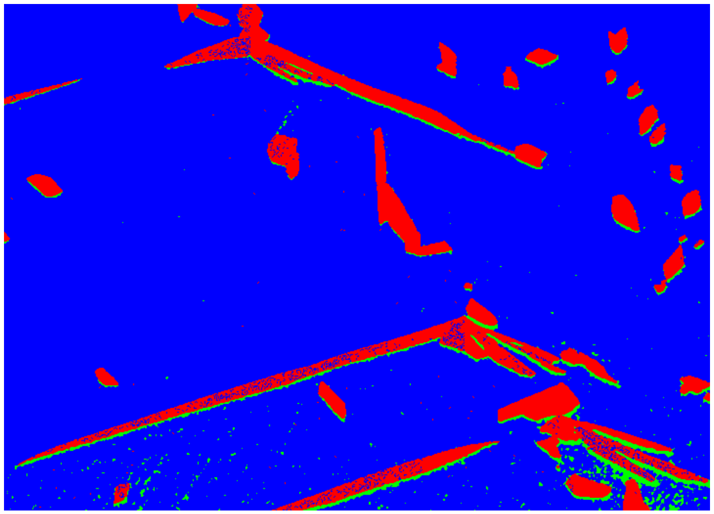

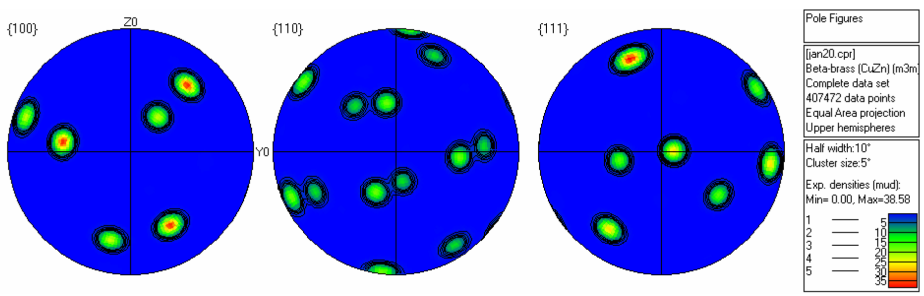

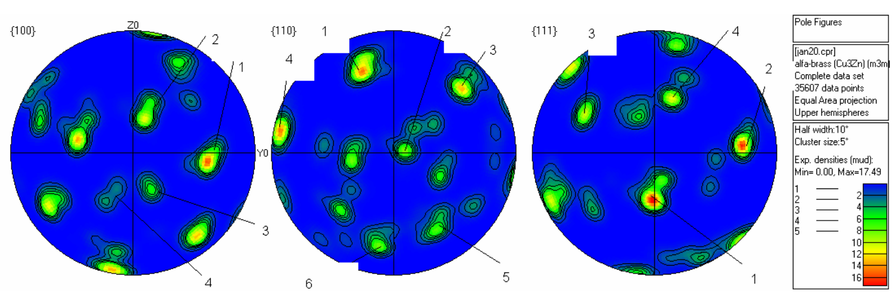

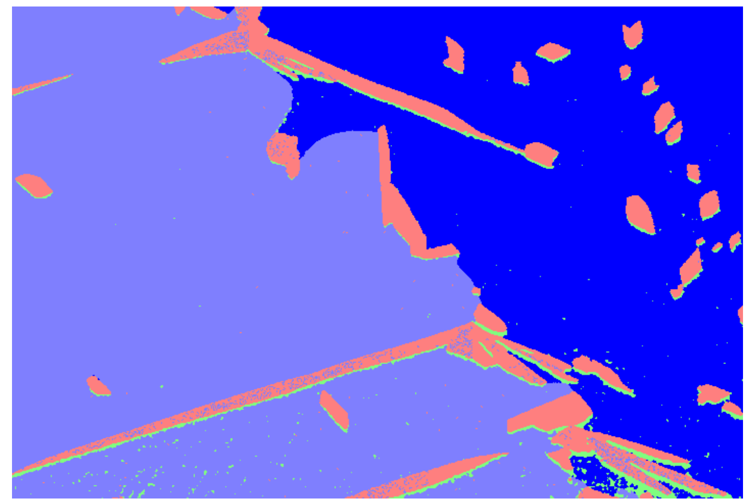

β orientation

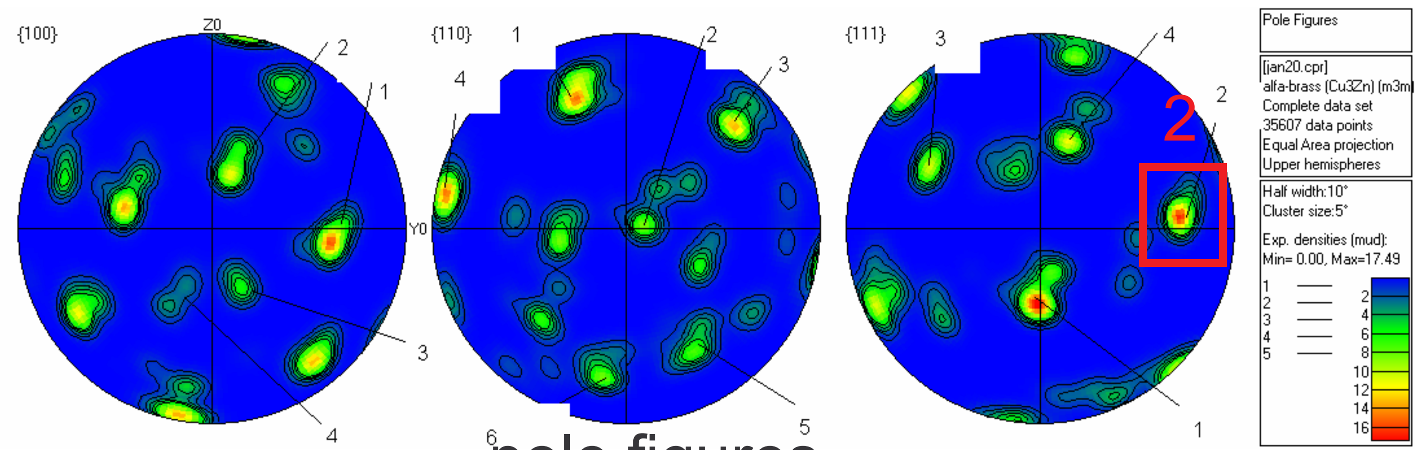

α pole figures

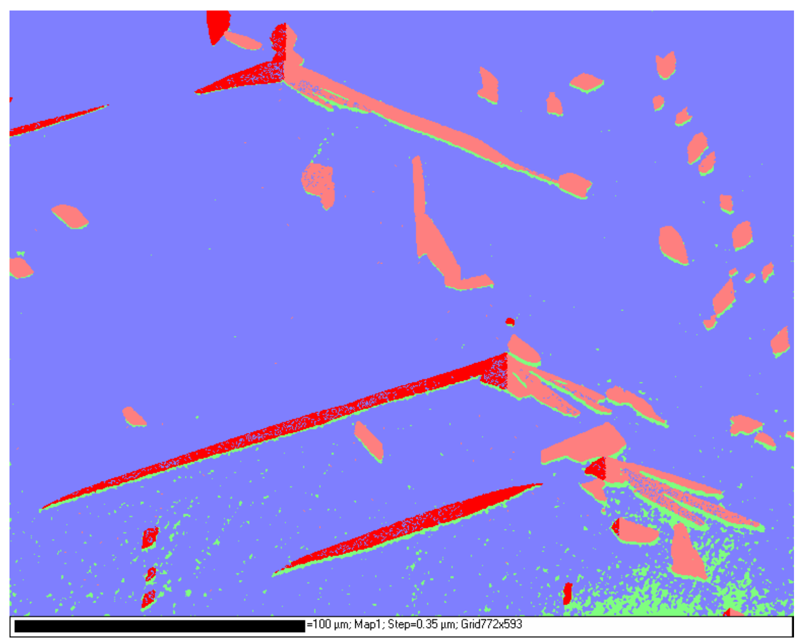

Image, (111)α maximum #2

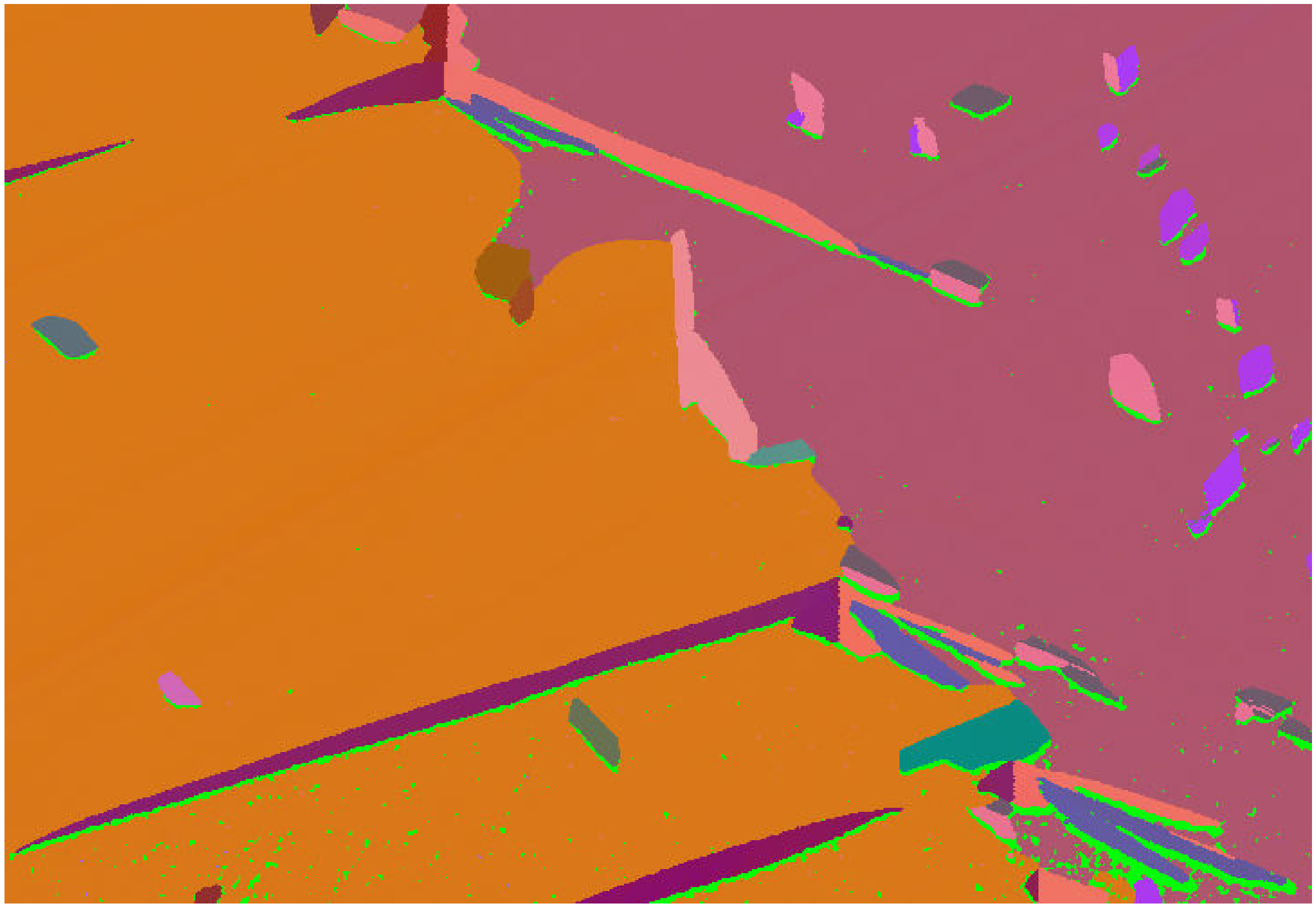

Composite image

For the future:

- complete kinetic studies and modelling of θ' growth in Al-Cu, and
- compare measurements with extended model.

- continue experimental study of grain-boundary-initiated Widmanst✍tten α from β brass (crystallographic and kinetic aspects), and
- continue phase-field modelling of kinetics in brass.

- extend studies to Bainite/ Widmanst✍tten ferrite in steels.

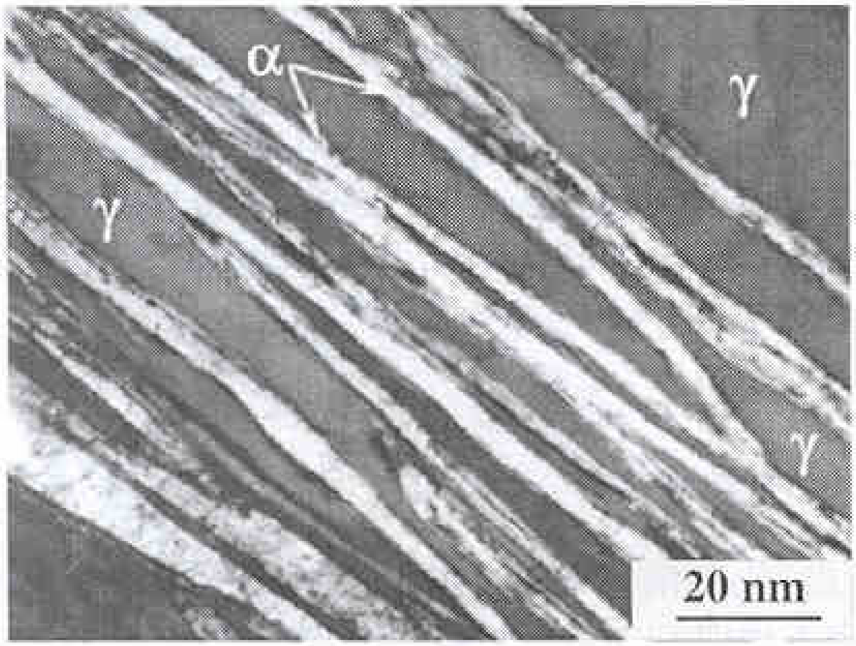

Fig. 5. Transmission electron micrographs of microstructure obtained at 200°C for 15 days in Steel B.

Bainite in Fe-1.0C-1.5Si-1.9Mn-1.3Cr-0.26Mo-0.1V, after Caballero and Bhadeshia, (2004).